

HiSST: 4th International Conference on High-Speed Vehicle Science Technology 22 -26 September 2025, Tours, France



Numerical analysis of combustion behind a strut injector within the LAPCAT-II chamber

G. Pelletier¹, N. Fdida², J. Labaune², S. Petit², G. Pilla², A. Vincent³, C. Pivard⁴, R. Santagata⁴, M. Scherman⁴,

Abstract

Reactive Reynolds-Averaged Navier-Stokes (RANS) simulations, using the CEDRE software, were conducted to investigate the combustion behavior resulting from fuel injection through a strut injector into a confined transverse supersonic flow of vitiated air. The corresponding experimental conditions were studied in the LAPCAT-II combustor, operating in the LAERTE facility at the ONERA Palaiseau Research Center. This study examines four distinct operating conditions, characterized by variations in stagnation temperature and equivalence ratio, covering a range from nominal combustion to regimes approaching thermal choking. The first condition serves as a reference case for validating the numerical methodology, through comparison with various experimental diagnostics, including pressure measurements, reaction zone position via OH* chemiluminescence, shock positions using Schlieren imaging, and single gas temperature measurement by CARS. Additionally, the stabilization mechanism of the flame under this condition is analyzed. The three others are used to study the appearance of thermal choking within the chamber.

Keywords: Supersonic Combustion; Strut injector; Scramjet; Hydrogen; thermal Choking; RANS simulation; Shock train

Nomenclature

Latin

k – turbulent kinetic energy (m²·s⁻²)

T – Temperature (K)

P - Pressure (Pa)

V – flow velocity (m·s⁻¹)

x, y, z – cartesian coordinates (mm)

Y – mass fraction (-)

Greek

 α – Relative to the species

 Φ – Equivalence ration (-)

 ω – Pseudo-dissipation (s⁻¹)

 $\dot{\omega}$ – Species production rate (s⁻¹)

HiSST-2025-26 Numerical analysis of combustion behind a strut injector within the LAPCAT-II chamber

¹ ONERA, Université Paris Saclay, F-91123 Palaiseau-France, DMPE-MPA

² ONERA, Université Paris Saclay, F-91123 Palaiseau-France, DMPE-LPA

³ ONERA, Université Paris Saclay, F-91123 Palaiseau-France, DMPE-MH

⁴ ONERA, Université Paris Saclay, F-91123 Palaiseau-France, DPHY-SLM

1. Set-up

The LAPCAT-II combustor is fed with a Mach 2 hot vitiated air-stream issued from a Laval nozzle. This vitiated air-stream is produced through a preliminary H2-air combustion, followed by oxygen replenishment to maintain an oxygen molar fraction of 0.21. The inlet stagnation temperature is adjustable within the range of 1300-1900 K, while the stagnation pressure can range from 0.1 MPa to 1.2 MPa.

The combustor features a constant width of 40 mm and consist of four consecutive sections. The initial section, serving as the isolator, has a uniform cross-sectional area with an inlet height of 35.4 mm and a length of 215 mm. It is followed by three additional sections with half angles of 1° (318 mm), 3° (354.5 mm), and again 1° (305 mm). These divergent geometries are designed to delay or prevent the onset of thermal choking within the chamber. The total length of the combustor, measured from the Laval nozzle exit to the end of the final divergent section, is 1257 mm. Large optical access windows are integrated along the combustor walls, enabling the use of advanced optical diagnostics. These include single-point CARS (Coherent Anti-Stokes Raman Scattering) measurements, as well as flow visualization techniques such as OH* chemiluminescence or Schlieren imaging, as well as planar laser-induced fluorescence (PLIF) [1]. Figure 1 presents the geometry of the Mach 2 Laval nozzle alongside the full combustor configuration, with the reference position x = 0 mm corresponding to the nozzle throat.

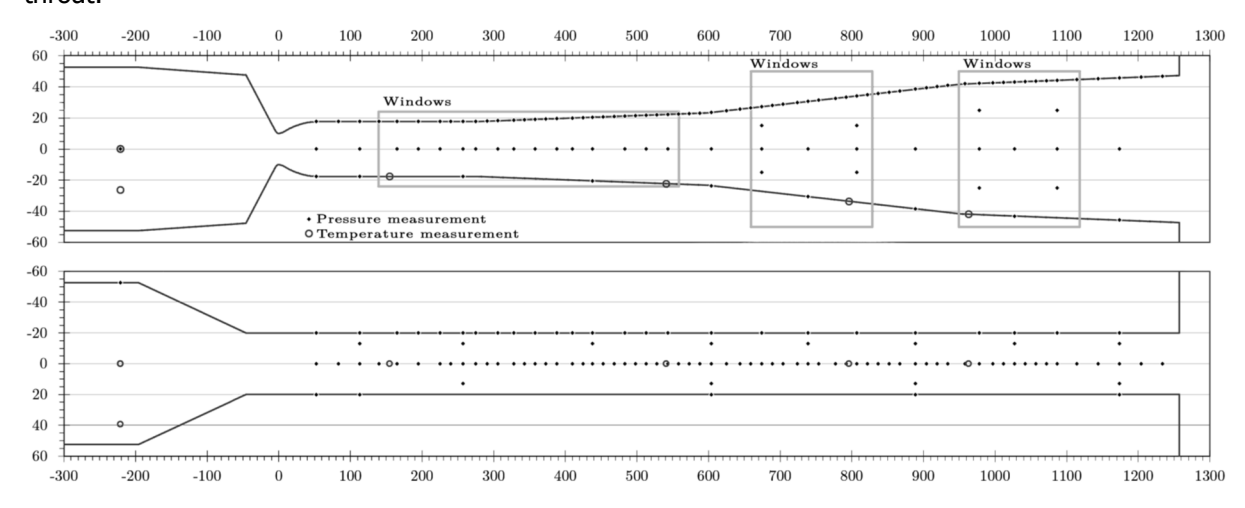


Figure 1 Geometry of the LAPCAT-II combustor

The combustion chamber is made of a copper alloy, with its inner walls coated by a 300 μ m thick thermal barrier coating (TBC) made of Yttria-stabilized Zirconia (where Yttria refers to yttrium oxide). The surface of the TBC exhibits a sandpaper-like texture, which has been characterized using scanning electron microscopy (SEM), yielding an average surface roughness of approximately 65 μ m.

Hydrogen is injected into the primary supersonic vitiated air stream via a strut injector, depicted in Figure 2. The strut is equipped with two injection ports, each 2 mm in diameter, located symmetrically on either side. These ports are positioned at x = 200 mm.

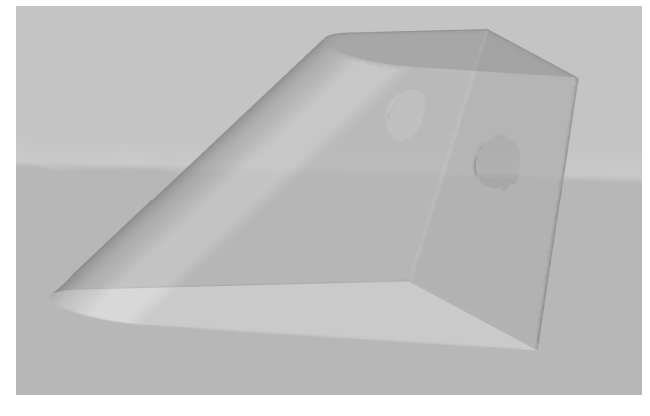


Figure 2 Geometry of the injection strut

Combustion within the LAPCAT-II combustor, using the aforementioned strut injector, has been investigated under four distinct operating conditions, summarized in Tableau 1. The effect of the inlet stagnation temperature T_0 is investigated via Case A and B, while cases B, C and D explore the influence of the global equivalent ratio Φ .

Tableau 1 Experimental conditions

| Ref. | T ₀ (K) | Ф |
|--------|--------------------|------|
| Case A | 1700 | 0.12 |
| Case B | 1400 | 0.12 |
| Case C | 1400 | 0.15 |
| Case D | 1400 | 0.2 |

2. Computational Model

This study is carried out using ONERA's computational fluid dynamics (CFD) platform CEDRE [2], a multi-physics environment designed for the simulation of complex flow phenomena via specialized solvers. Specifically, this study harnesses the capabilities of the finite volume three-dimensional compressible and reactive Navier-Stokes solver CHARME.

Reynolds-averaged Navier-Stokes (RANS) numerical simulations are performed within the framework of Menter's $k-\omega$ shear stress transport (SST) turbulence model [3]. The Reynolds fluxes of mass and energy deduced from the turbulent diffusivity approximation by introducing turbulent Schmidt and Prandtl numbers, which are set to a conventional value of 0.9 [4]. This turbulence model is used in conjunction with a wall roughness model [5] , which is particularly important in this context as it accounts for the residual surface roughness of the thermal barrier coating (TBC), a critical parameter for accurately reproducing the experimental observations [6-8].

The averaged chemical source terms $\bar{\omega}_{\alpha}$ in the species transport equations are modeled using the Well-Stirred Reactor (WSR) approach. This framework assumes that subgrid-scale fluctuations in composition are negligible at the resolved level, such that $\bar{\omega}_{\alpha} = \dot{\omega}_{\alpha}(\tilde{T}, \tilde{Y}_{\alpha})$. This assumption is widely used in high-speed combustion simulations [9-12]. The chemical reaction rates are computed based on the detailed kinetic mechanism developed by Jachimowski [13].

3. Numerical Results

3.1. Comparisons to the experimental results

To evaluate the accuracy of the numerical simulations, the computational results are compared against multiple experimental measurements. Local static pressure data, acquired along the upper wall of the combustion chamber, as well as gas temperature CARS measurements, are directly compared with the corresponding numerical predictions. Additionally, visualizations from the experiments are compared to their numerical counterparts, synthetic Schlieren fields, estimated from the norm of the density gradient, and heat release rate integrated across the full width of the chamber.

3.2. Pressure measurements

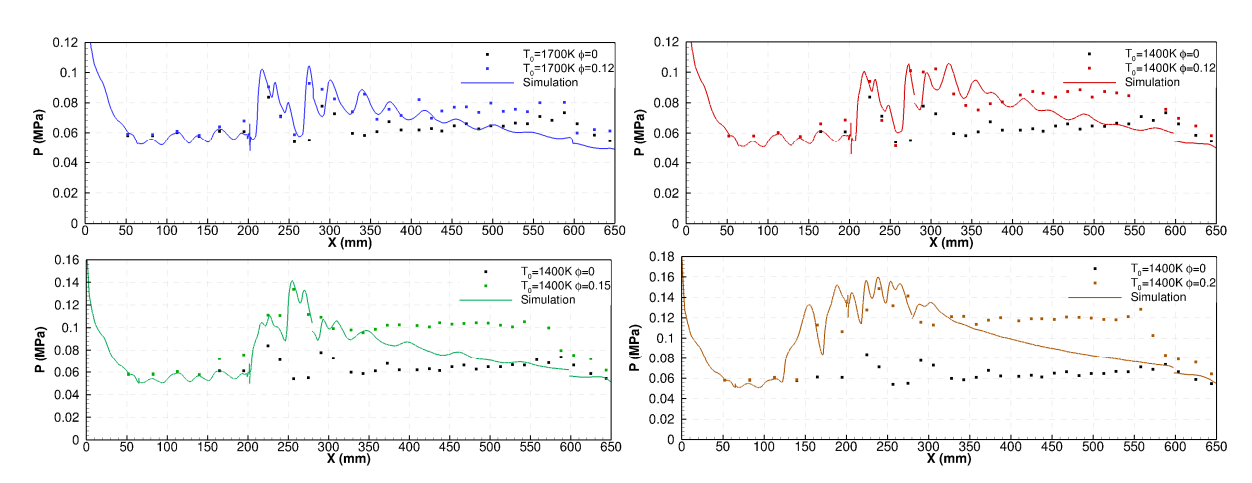


Figure 3 Wall pressures levels for case A to D

The comparisons to pressure measurements for each set of experimental condition is presented on Figure 3. For each condition, black dots refer to the pressure profile recorded in non-reactive conditions (no injection of H2), while colored dots are the the reactive case. Profiles A, B and C reveal a series of successive peaks downstream of the injection strut, located at x=200mm. These peaks result from shock reflections on the chamber walls, as illustrated by the Schlieren visualizations in Figure 4. These peaks are rapidly followed by the combustion development, which leads to a rise in global pressure levels observable in the region 250<x<350mm, a shown in Figure 5. In contrast, Case D exhibits a pressure rise upstream of the injection strut located at x=130mm in the simulations and between x=140and x=160mm in the experiments. This behavior is indicative of thermal choking occurring within the chamber [14]. The observed discrepancies between numerical and experimental results in this region may be attributed to several modeling limitations, including the choice of turbulence model, the combustion representation, or the lack of detailed turbulence-chemistry interaction (TCI) modeling. Further downstream (x>350mm), the simulations and experiments diverge in their predicted pressure trends. While the numerical results show a gradual pressure decrease, consistent with the chamber's divergent geometry, the experimental data reveal a pressure plateau that remains unexplained. This plateau behavior has also been observed in other pressure measurements conducted in the LAPCAT-II combustor [6-8], suggesting a recurring feature whose origin has yet to be convincingly interpreted.

3.3. Visualizations comparisons

Schlieren and OH* chemiluminescence imaging were performed for all four operating conditions. The corresponding numerical visualizations were generated using two approaches: a numerical Schlieren field derived from the density gradient along the streamwise direction, and the heat release rate (HRR) integrated across the full width of the combustor. The dark thick line located above the strut on the Schlieren images on Figure 4 results from deposit on the windows. The comparisons between experimental and numerical visualizations are presented in Figure 4 and Figure 5. For Cases A, B, and D, the shock structures induced by the strut injector are well captured by the simulations. In particular, reflected shocks in the vicinity of the combustion ignition region are accurately reproduced. In Case C, a shock structure is also observed upstream of the strut, both in experiments and simulations. This case approaches the thermal choking limit, making it especially sensitive to the modeling strategy. The numerical simulation appears to trigger early manifestations of choking under these conditions. OH* comparisons, shown in Figure 5, demonstrate a satisfactory agreement between experiments and simulations in terms of flame location and structure for all four cases. For Cases B, C, and D, both the experimental OH* signal and the simulated HRR indicate a progressive increase in combustion intensity with rising equivalence ratio, suggesting that a greater amount of hydrogen is burned in the same region as fuel availability increases.

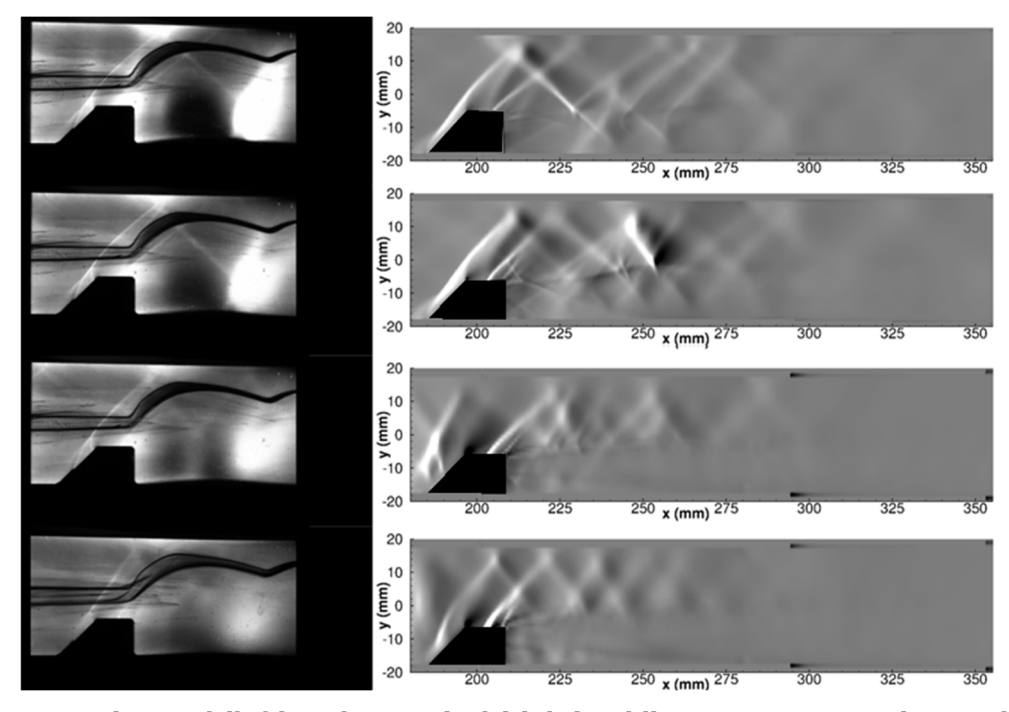


Figure 4 Experimental (left) and numerical (right) Schlieren. Case A to D (Top to bottom)

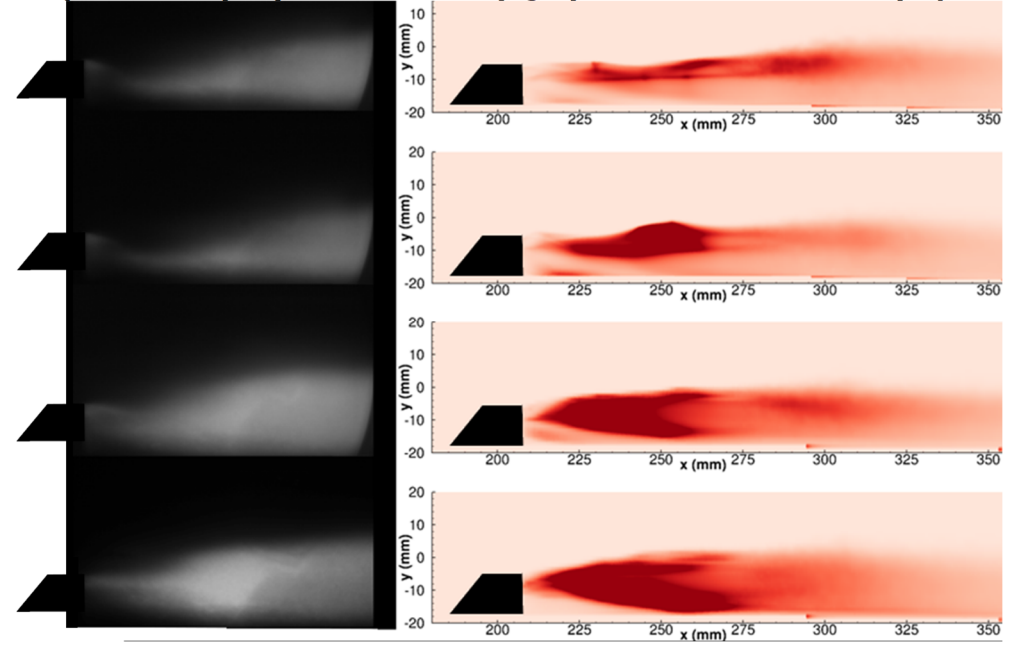


Figure 5 OH* chemiluminescence (left) and Heat Release Rate (right). Case A to D (Top to bottom)

3.4. Temperature measurements

CARS temperature measurements were carried out along the lines indicated in Figure 6. This diagnostic technique, previously validated under other LAPCAT-II injection conditions [15] is employed here to provide detailed thermodynamic insight. Comparisons with simulation results are presented for Case 1 only. The measurement lines were selected to probe both the incoming freestream and the combustion development downstream of the strut injector. In particular, one streamwise line upstream of the injector (i.e line 1) captures the thermal state of the vitiated air prior to fuel injection, thus characterizing the inlet conditions impinging on the hydrogen jet. Additionally, three vertical lines (2, 3 and 4) positioned downstream of the strut are used to probe vertical evolution of combustion along the flow path. Two horizontal lines (5 and 6) were also investigated. The first, located in the mid-height of the chamber, lies outside the core combustion region and primarily reveals temperature peaks associated with shock structures. The second, aligned with the elevation of the injection holes, traverses the main

HiSST-2025-26 Page | 5 Numerical analysis of combustion behind a strut injector within the LAPCAT-II chamber

combustion zone, offering direct insight into flame development and heat release. The CARS setup exploited in this experiment emits 1kHz trains of pulses enabling up to kHz measurements of the temperature within a cylinder shape of approximatively 0.1 mm in diameter and 1.5 mm long. N2 CARS spectra were acquired at a rate of 100 Hz (10-shot integration) for line 1, and at 10 Hz (100-shot integration) for the remaining lines.

| Reference | x (mm) | y (mm) | z (mm) | Frequency (Hz) |
|-----------|------------------------|----------|--------|----------------|
| 1 | 171 | Variable | 0 | 100 |
| 2 | 10 mm downstream strut | Variable | 0 | 10 |
| 3 | 80 mm downstream strut | Variable | 0 | 10 |
| 4 | 290 | Variable | 0 | 10 |
| 5 | Variable | 0 | 0 | 10 |
| 6 | Variable | -8 | 0 | 10 |

Table 2. CARS measurements lines

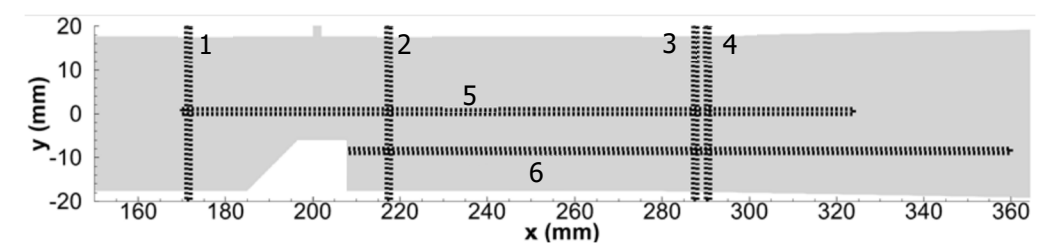


Figure 6 CARS Measurements lines

The comparison between simulation results and experimental CARS temperature measurements is presented in Figure 7. A satisfactory agreement is observed for vertical lines 2, 3, and 4, particularly from the upper part of the flowfield down to the region where a temperature rise is detected, corresponding to the onset of combustion. However, for line 3, notable discrepancies appear near the lower wall, a region not shown for lines 2 and 4 due to the absence of experimental data. This behaviour is particularly intriguing, given the low flow velocity in this area and the presence of active combustion, as evidenced by OH* chemiluminescence in the corresponding visualizations.

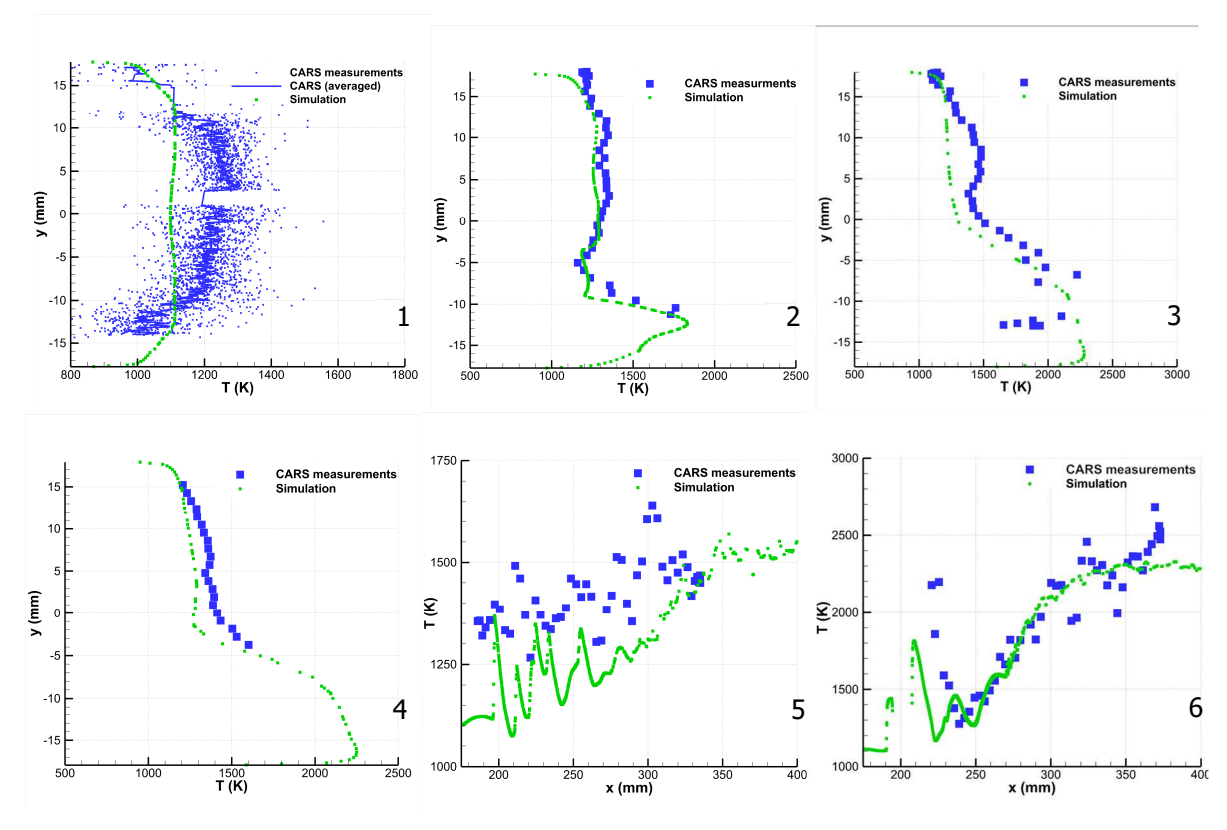


Figure 7 Comparison to CARS measurements along the corresponding line

Temperature measurements upstream the strut (i.e. line 1) reveal a distribution that deviates slightly from the numerical predictions. Specifically, the experimental data show higher temperatures in the freestream core and lower temperatures near the walls, whereas the numerical simulations assume a uniform inlet temperature profile. This discrepancy is attributed to the simplified thermal boundary condition at the inlet, which assume the temperature as uniform. A similar trend has previously been observed with TDLAS measurements [6] in other experimental campaigns conducted on the LAERTE facility. Although refining the inlet temperature profile could improve agreement in the upstream region, such refinement is not deemed critical for the current study, as combustion in this configuration is not governed by auto-ignition. Along line 5, a temperature offset of approximately 200 K is observed between simulations and CARS measurements. This offset is consistent with the mismatch observed at the mean axial location on line 1. Nevertheless, the position of the temperature peaks is accurately reproduced. The final measurement line 6, analysed shows excellent agreement between experimental and numerical temperature profiles. This consistency suggests that the combustion process is well captured by the numerical model under the investigated conditions.

3.5. Description of the flow

To further analyze the internal flow dynamics, Case A is examined in greater detail. The most prominent feature in this configuration is the strut injector, which supplies fuel to the combustor. This geometric protrusion, positioned within the supersonic crossflow, generates a system of shock waves that propagate and reflect within the chamber. Figure 8 presents numerical Schlieren visualizations, integrated either along the width or the height of the combustor. These images clearly show the shock structures originating from the strut and their subsequent reflections on both the top and side walls of the chamber. Notably, reflected shocks intersect the hydrogen mixing layer at approximately x=230, 245 and 260mm. These shock-mixing layer interactions play a crucial role in promoting ignition and supporting combustion stabilization of the injected fuel.

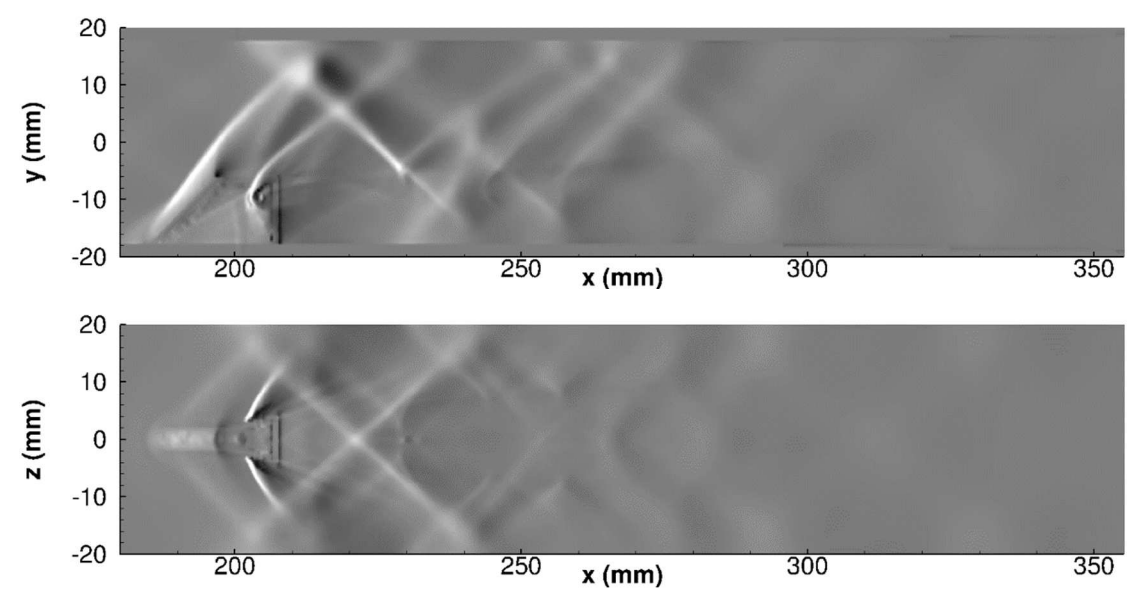


Figure 8 Numerical Schlieren of case A integrated along the width (top) and height (bottom) of the combustor

Figure 9 illustrates the hydrogen mixing process through cross-sectional planes located at x=[108; 215;225; 250]mm shows the atomic equivalence ratio, showing the distribution of the atomic equivalence ratio. The geometry of the strut, combined with the flow characteristics typical of a Jet in Supersonic Crossflow (JISC), promotes the development of a distinct vortical topology, namely a counter-rotating vortex pair (CVP). These vortices are clearly visible in the figure through streamlines superimposed on the equivalence ratio contours. Near the injection ports, the CVP gradually transports the hydrogen downstream in the vicinity of the strut. Further downstream, the vortices begin to merge, resulting in a broader and more uniform distribution of the fuel in the far field.

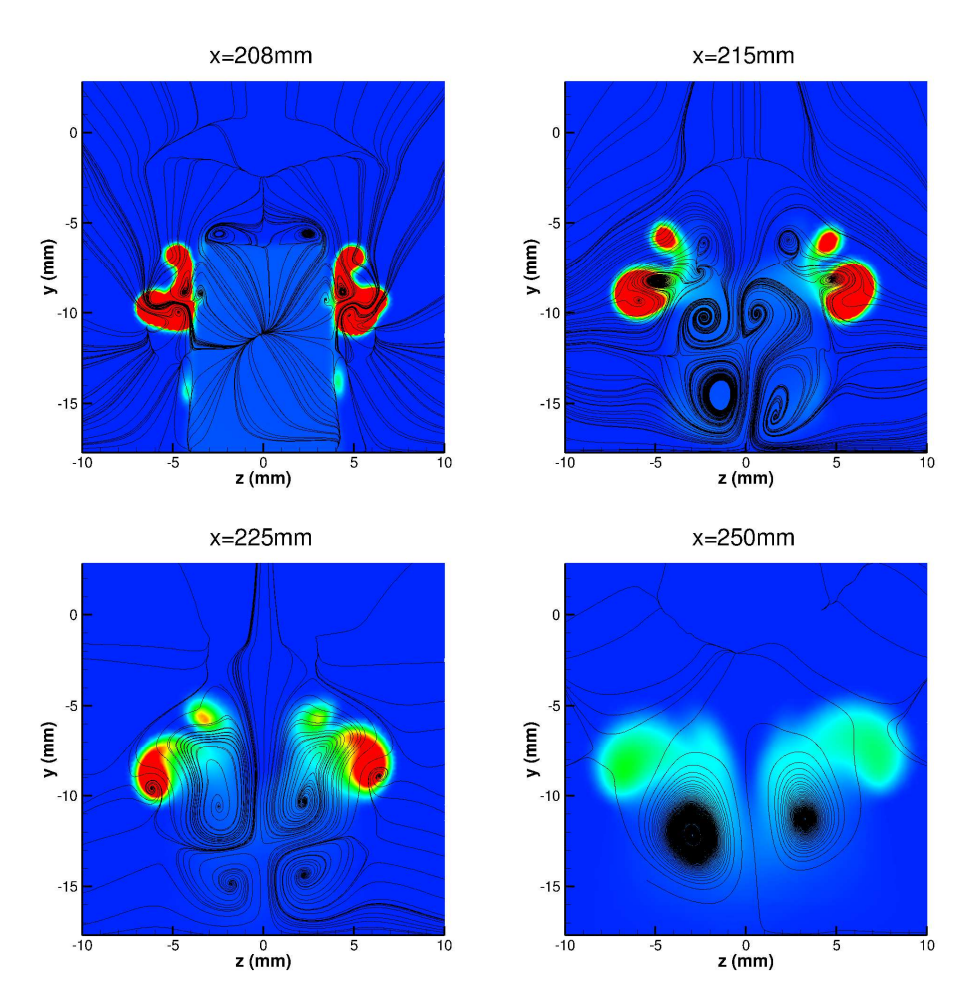


Figure 9 Streamlines superimposed to equivalence ratio contour downstream the strut

A recirculation region, identified through velocity contours shown in Figure 10 forms and stabilizes immediately downstream of the injection strut. This low-velocity zone plays a crucial role in initiating combustion. The influence of this recirculation is further evidenced in Figure 11 which displays elevated temperature levels in the same region, consistent with the reduced flow velocity.

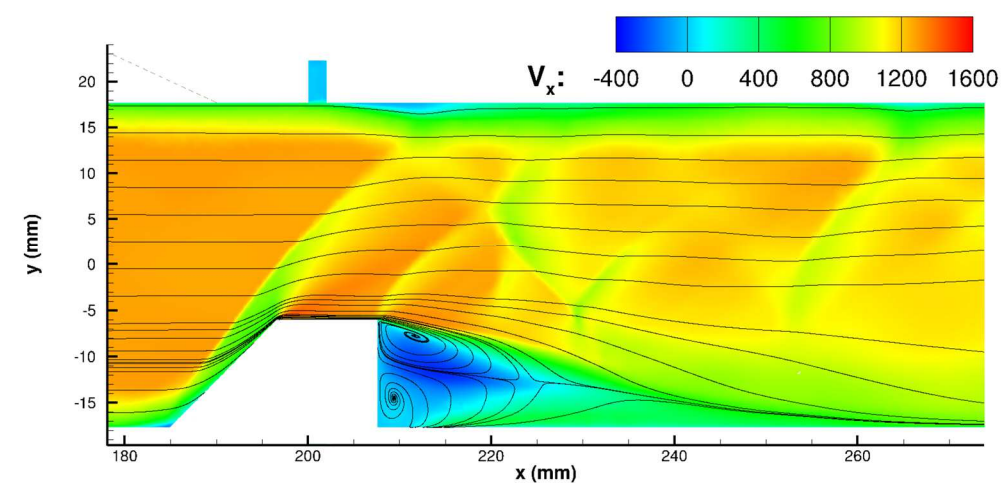


Figure 10 Velocity contour with streamlines in the plane z=0

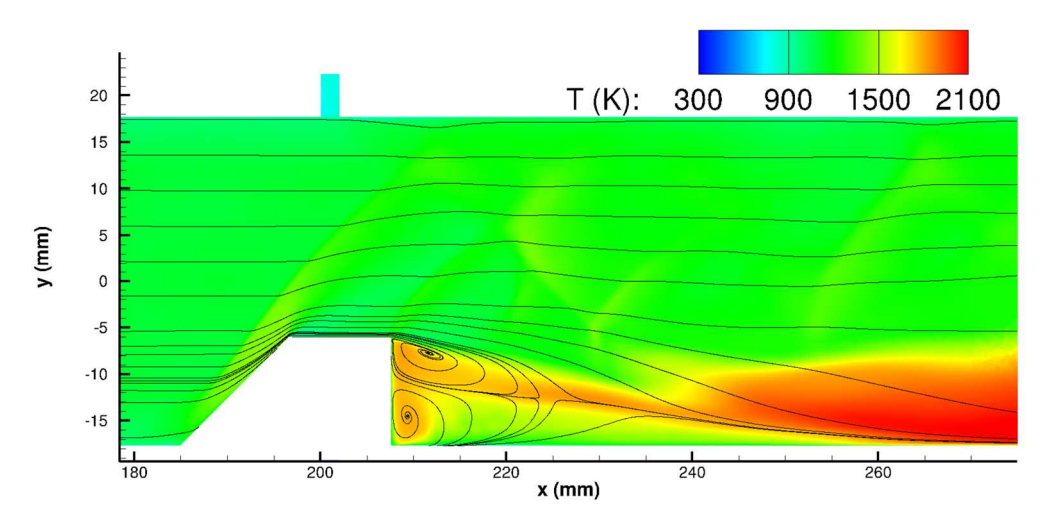


Figure 11 Temperature contour with streamlines in the plane z=0

3.6. Analysis of the combustion ignition

The role of shock waves in combustion ignition is emphasized in Figure 12 which shows that regions of maximum heat release rate (HRR) coincide with the locations where shocks reflect onto the hydrogen mixing layer observable on Figure 13. To further illustrate this mechanism, Figure 14 presents the longitudinal gradient of the HRR, highlighting areas where the heat release increases sharply. Four distinct regions of elevated HRR gradient are identified. The first three correspond to positions where reflected shocks intersect the fuel—air mixing layer, confirming their direct contribution to ignition. The fourth region aligns with the interface between the downstream recirculation zone and the incoming fresh gases, indicating that this recirculation bubble plays a secondary role by anchoring the flame once ignition has been initiated. These observations suggest that, under the present combustion regime, shock reflections act as the primary ignition mechanism, while the recirculation zone stabilizes the flame and supports sustained combustion.

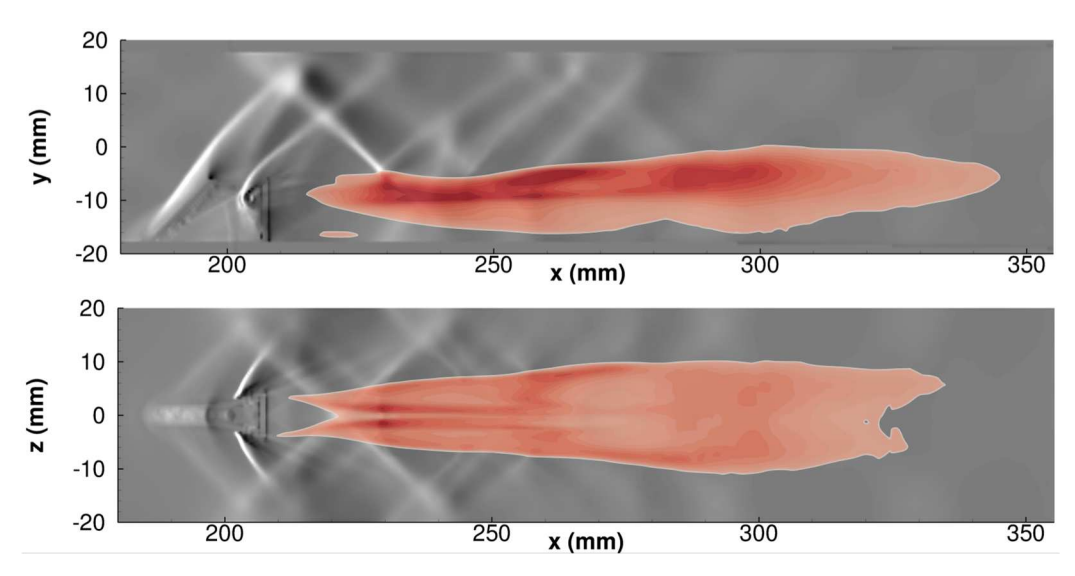


Figure 12 Numerical Schlieren and HRR superimposed integrated along the width (top) and the height (bottom) of the combustor

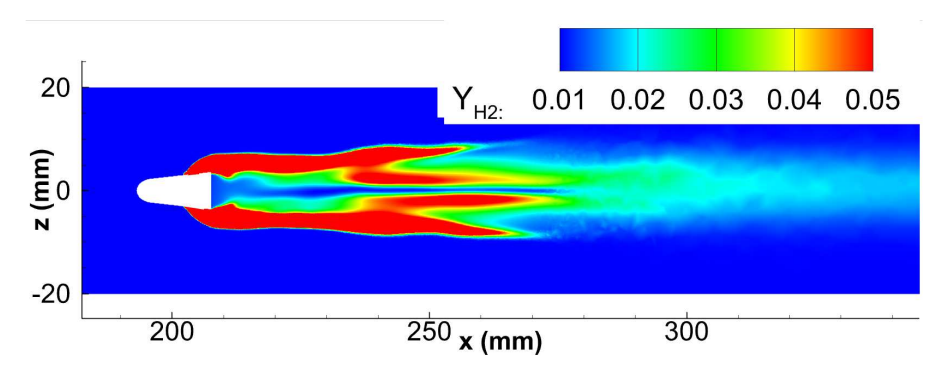


Figure 13 Hydrogen mass fraction contour in the y-plane located at the injection height

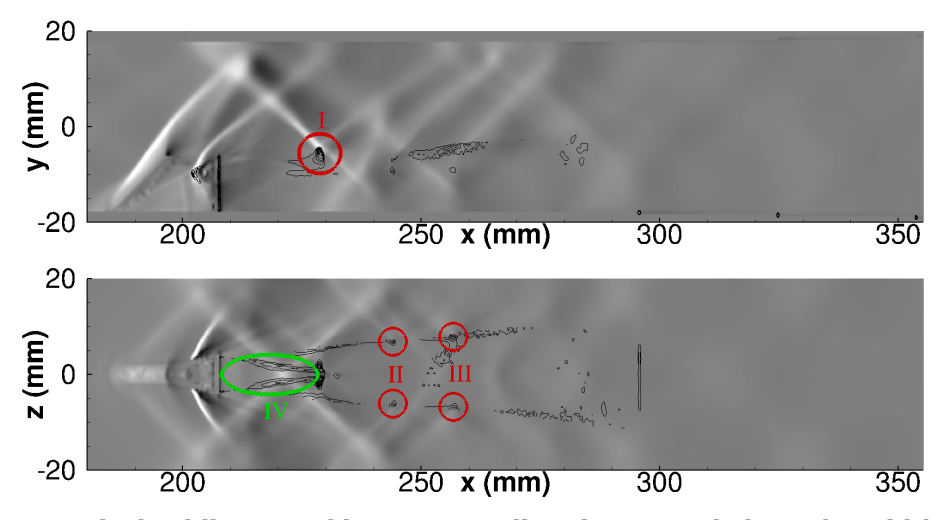


Figure 14 Numerical Schlieren and iso-HRR gradient integrated along the width (top) and the height (bottom) of the combustor

3.7. Analysis of the thermal choking of the chamber

Thermal choking in the combustor is investigated through the comparison of Cases B, C, and D, in which the equivalence ratio is progressively increased while maintaining a constant stagnation temperature. As previously shown in Figure 3, this leads to a rise in pressure downstream of the strut, associated with an increase in heat release rate (HRR). The resulting pressure buildup initiates the formation of shock structures upstream of the strut, a phenomenon analogous to shock trains observed in supersonic inlets. This behavior is captured in Figure 15. The position and intensity of these shocks are driven by the equivalence ratio, and in extreme cases, may lead to nozzle unstart, marking the onset of thermal choking. This set of experimental conditions provides a valuable framework for calibrating and validating numerical models, ensuring that they accurately capture the combustion, shock structures, and flow choking within the chamber.

HiSST-2025-26

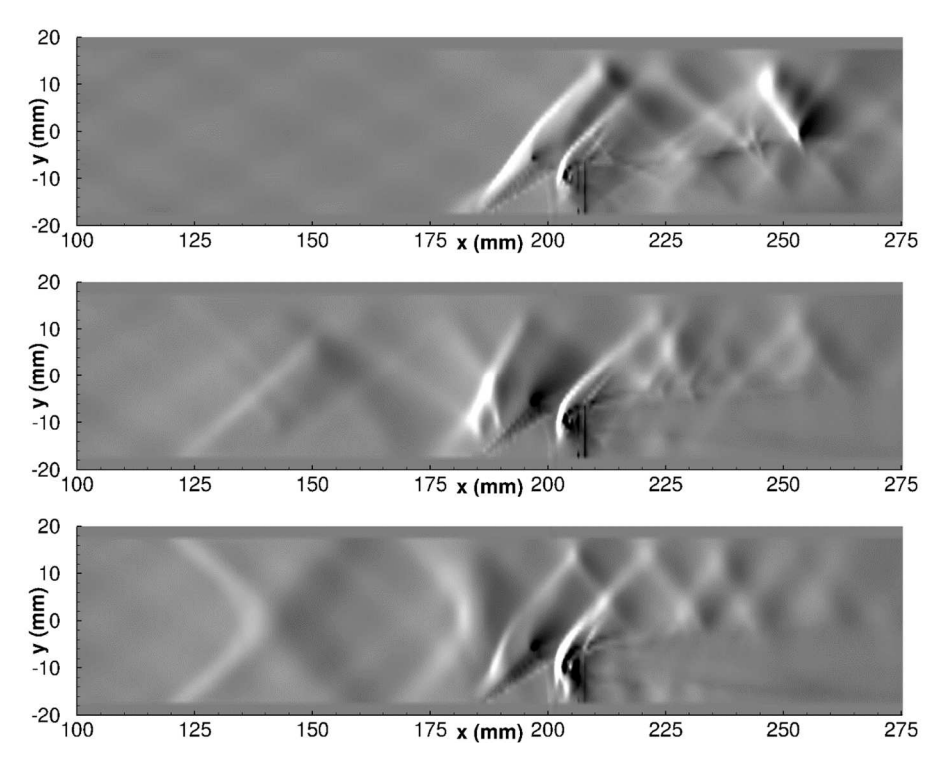


Figure 15 Numerical Schlieren upstream the strut for cases B, C and D

4. Conclusion

This study has presented a detailed numerical investigation of reactive supersonic combustion in the LAPCAT-II combustor, using Reynolds-Averaged Navier—Stokes (RANS) simulations performed with ONERA's CEDRE code and the CHARME solver. The numerical results were compared against a comprehensive set of experimental data acquired in the LAERTE facility, including pressure measurements, OH* chemiluminescence, Schlieren visualizations, and CARS temperature measurements.

Four operating conditions, covering a range of equivalence ratios and combustion regimes—from nominal operation to near thermal choking—were examined. The simulation results show good agreement with experimental data in terms of pressure evolution, flame structure, and temperature fields, particularly for the nominal case (Case A). The contribution of shock reflections to combustion ignition and the role of the recirculation zone in flame stabilization were clearly identified through numerical Schlieren fields and HRR gradients.

The formation of thermal choking was analyzed through cases B to D, highlighting how increased equivalence ratios lead to elevated downstream pressure and upstream shock formation, consistent with shock train behavior. These effects were shown to be sensitive to local flow structures and combustion—turbulence interaction, underlining the importance of accurate modeling strategies.

Overall, this work demonstrates that numerical tools, when properly calibrated, can reliably capture the key physical mechanisms governing supersonic combustion in complex geometries. The insights gained from this study offer a strong foundation for further development and optimization of predictive models, particularly regarding shock-induced ignition, mixing processes, and flame holding in high-speed propulsion systems.

HiSST-2025-26 Page |

References

- 1. Ristori, A., Brossard, C., and Vincent-Randonnier, A., "Diagnostics optiques des écoulements supersoniques dans une chambre de combustion de statoréacteur mixte au moyen de la strioscopie à haute cadence couplée à la visualisation de l'émission du radical OH*," CFTL 2016, Toulouse, France, 2016
- 2. Refloch, A., Courbet, B., Murrone, A., Villedieu, P., Laurent, C., Gilbank, P., Troyes, J., Tessé, L., Chaineray, G., Dargaud, J.-B., Quémerais, E., and Vuillot, F.: CEDRE Software. AerospaceLab Journal, 1–10 (2011)
- 3. Menter, F., "Two-Equation Eddy-Viscosity Transport Turbulence Model for Engineering Applications," AIAA Journal, Vol. 32, No. 8, 1994, pp. 1598–1605. 10.2514/3.12149
- 4. Launder, B. E., and Sharma, B. I., "Application of the Energy-Dissipation Model of Turbulence to the Calculation of Flow Near a Spinning Disc," Letters in Heat and Mass Transfer, Vol. 1, No. 2, 1974, pp. 131–138. 10.1016/0094-4548(74)90150-7.
- 5. Aupoix, B.: Roughness Corrections for the k- ω Shear Stress Transport Model: Status and Proposals. J. Fluids Eng. (2015). <u>10.1115/1.4028122</u>.
- 6. G. Pelletier, G. Vilmart, A. Vincent-Randonnier and C. Brossard, "Numerical characterization of the LAERTE intake flowfield and effect on combustion", 25th AIAA International Space Planes and Hypersonic Systems and Technologies Conference, 2023.
- 7. Vincent-Randonnier, A., Moule, Y., and Ferrier, M., "Combustion of Hydrogen in Hot Air Flows within LAPCAT-II Dual Mode Ramjet Combustor at Onera-LAERTE Facility Experimental and Numerical Investigation," AIAA Paper 2014-2932, 2014. https://doi.org/10.2514/6.2014-2932.
- 8. Pelletier, G., Ferrier, M., Vincent-Randonnier, A., Sabelnikov, V., and Mura, A.: Wall Roughness Effects on Combustion Development in Confined Supersonic Flow. J. Propuls. Power (2020). https://doi.org/10.2514/1.B37842
- 9. Desornes, O., and Scherrer, D., "Tests of the JAPHAR Dual Mode Ramjet Engine," Aerospace Science and Technology, Vol. 9, No. 3, 2005, pp. 211–221. https://doi.org/10.1016/j.ast.2005.01.007.
- 10. Potturi, A. S., and Edwards, J. R., "Large-Eddy/Reynolds-Averaged Navier-Stokes Simulation of Cavity-Stabilized Ethylene Combustion," Combustion and Flame, Vol. 162, No. 4, 2015, pp. 1176–1192. https://doi.org/10.1016/j.combustflame.2014.10.011.
- 11. Fulton, J. A., Edwards, J. R., Cutler, A., McDaniel, J., and Goyne, C., "Turbulence/Chemistry Interactions in a Ramp-Stabilized Supersonic Hydrogen-Air Diffusion Flame," Combustion and Flame, Vol. 174, 2016, pp. 152–165. https://doi.org/10.1016/j.combustflame.2016.09.017.
- 12. Candler, G. V., Cymbalist, N., and Dimotakis, P. E., "Wall-Modeled Large-Eddy Simulation of Autoignition-Dominated Supersonic Combustion," AIAA Journal, Vol. 55, No. 7, 2017, pp. 2410–2423. https://doi.org/10.2514/1.
- 13. Jachimowski, C.: An Analysis of Combustion Studies in Shock Expansion Tunnels and Reflected Shock Tunnels. NASA-TP-3224. (1992).
- 14. Susumu Mashio, Keiichi Kurashina, Takahiro Bamba, Shingo Okimoto and Shojiro Kaji. "Unstart phenomenon due to thermal choke in scramjet module," AIAA 2001-1887. *10th AIAA/NAL-NASDA-ISAS International Space Planes and Hypersonic Systems and Technologies Conference*. April 2001.
- 15. Pivard, C., Scherman, M., Santagata, R. *et al.* High-speed fs/ps-CARS thermometry for supersonic H₂/air combustion studies. *Exp Fluids* **66**, 79 (2025). https://doi.org/10.1007/s00348-025-04007-y

HiSST-2025-26 Page |